Supporting Information for
Analysis of Optical Activity in Terms of Bonds and Lone-Pairs: The Exceptionally Large Optical Rotation of Norbornenone

Barry Moore II,[a] Monika Srebro,[a,b] and Jochen Autschbach[a]*

[a] Department of Chemistry

University at Buffalo, State University of New York

Buffalo, NY 14260–3000

[b] Department of Theoretical Chemistry

Faculty of Chemistry, Jagiellonian University

R. Ingardena 3, 30–060 Krakow, Poland

* Corresponding author. Email: jochena@buffalo.edu.

October 20, 2012

The following information is provided in this document:

- Details of the OR analysis protocol adopted in the present work.
- Results of basis set incompleteness and origin dependence of the OR study with aug-cc-pVDZ basis set (Tables S1, S2, and S3).
- Details of optimal tuning of the PBE-based range-separated hydrid along with chiroptical data for the 'tuned' set of functionals (Figure S1, Table S4).
- Additional calculated data for the analysis of the OR for norbornenone including:
  - Composition of σ bonds involving carbons bridging C=O and C=C chromophores (Table S5).
  - LMO plots for selected important MOs of norbornenone (Figure S2).
  - Diagonal components of the optical rotation tensors at the static and dynamic (Na D-line) limit for various methods (Table S6).

- Plots of chiroptical response tensor for various methods at static limit (Figure S3).
- Principal axis 33 direction of the chiroptical response tensor for different views of norbornenone utilized in the present work (Figure S4).
- Selected dominant CMO and LMO contributions to β_{33} for various methods at static limit and Na D-line (Tables S7 and S8).
- Series of plots depicting selected dominant CMOs and LMOs, their electric-field and magnetic-field perturbations for the field oriented along the 33 direction, and the product of the perturbations (Figures S5, S6, S7, S8, S9, S10, S11, and S12).
- Comparison of LMO contributions to the OR of norbornenone and α-pinene at the static limit (Table S9 and Figure S13).
- Rotational analysis of norbornenone molecular fragment (Figure S14).

Analysis Protocol: Details

The isotropic optical activity observed for a solution of chiral molecules is determined by an imbalance in the cancellation of optical rotation tensor elements that are typically of opposing signs and sometimes have different orders of magnitude. It is therefore important to establish a theoretical setup that allows for a meaningful discussion of optical rotation tensor elements for different relative orientations of the molecule and the field direction of the linearly polarized electromagnetic wave. Atomic units are used through most of this section.

Following the discussion of Reference 1, the optical rotation parameter measured in the direction of a normalized directional vector $\boldsymbol{n}$ (defined in the laboratory coordinate system) is

$$\beta_{\boldsymbol{n}} = \boldsymbol{n} \cdot \tilde{\mathbb{B}} \boldsymbol{n} \tag{1}$$

where the elements ($\alpha, \beta \in \{x, y, z\}$) of the rank-2 tensor $\tilde{\mathbb{B}}$ can be written as

$$\tilde{B}_{\alpha\beta} = \frac{1}{2}\big[\,\mathrm{tr}[\mathbb{B}]\delta_{\alpha\beta} - B_{\alpha\beta})\big] \tag{2}$$

(which is a compact notation for the tensor derived in Reference 2). In the previous equation, $\delta_{\alpha\beta}$ is the Kronecker delta, and Greek indices indicate Cartesian coordinates. The tensor $\mathbb{B}$ is the origin-independent Buckingham-Dunn (BD) optical rotation tensor, with elements

$$B_{\alpha\beta} = \frac{1}{2}\left[\beta_{\alpha\beta} + \beta_{\beta\alpha} + \frac{1}{3}\sum_{\gamma,\delta}(\varepsilon_{\alpha\gamma\delta} A_{\gamma,\delta\beta} + \varepsilon_{\beta\gamma\delta} A_{\gamma,\delta\alpha})\right] \tag{3}$$

Assuming exact (nonrelativistic) wavefunctions for the ground state (ψ_0) and the electronic excited states (ψ_j), the quantities in Equation (3) are given by

$$\beta_{\alpha\beta} = 2\sum_{j\neq 0} \mathrm{Im}\, \frac{\langle\psi_0|\hat{\mu}_\alpha|\psi_j\rangle\langle\psi_j|\hat{m}_\beta|\psi_0\rangle}{\omega_j^2 - \omega^2} \tag{4}$$

$$A_{\alpha,\beta\gamma} = 2\sum_{j\neq 0} \omega_j\, \mathrm{Re}\, \frac{\langle\psi_0|\hat{\mu}_\alpha|\psi_j\rangle\langle\psi_j|\hat{\Theta}_{\beta\gamma}|\psi_0\rangle}{\omega_j^2 - \omega^2} \tag{5}$$

and the ε are elements of the Levi-Civita tensor. The symbols $\beta_{\alpha\beta}$ and $A_{\alpha,\beta\gamma}$ denote elements of the frequency-dependent optical rotation tensor $\mathbb{\beta}$ and the electric dipole – electric quadrupole polarizability tensor $\mathbb{A}$, respectively. Both are calculated for the electronic ground state. The one-electron transition moment operators in Equation (4) and (5) are the electric dipole $\hat{\mu}_\alpha = -r_\alpha$, magnetic dipole $\hat{m}_\beta = -\frac{1}{2}(\boldsymbol{r}\times\hat{\boldsymbol{p}})_\beta$, and traceless electric quadrupole operator $\hat{\Theta}_{\beta\gamma} = -\frac{1}{2}(3r_\beta r_\gamma -$

$\delta_{\beta\gamma} r^2$), summed over all electrons, where $\boldsymbol{r}$ is an electron coordinate, r is the length of $\boldsymbol{r}$, and r_α is one of the vector components. Further, ω_j are electronic excitation frequencies and ω is the frequency of the electromagnetic wave interacting with the molecule. The definitions given here for the BD tensor and for the orientation-dependent optical rotation are for the off-resonance case where ω does not coincide with one of the excitation frequencies. For further details and extensions of the formalism to the near-resonance case, see References 3, 4, and 5.

Basis set incompleteness, and origin dependence of the optical rotation

In our calculations, exact ground- and excited-states wavefunctions are not available. Instead, the respective tensor elements are calculated using linear response time-dependent DFT (TDDFT). For details, see References 6 and 7. In this context it is worthwhile mentioning that the elements of the tensor $\mathbb{\beta}$ are not origin invariant even in exact theory. Only in conjunction with the dipole-quadrupole tensor are origin invariant optical activity tensor elements obtained, hence the construction of $\tilde{\mathbb{B}}$ from the BD tensor. However, this requires that the calculations do not introduce an additional spurious origin dependence of the tensor $\mathbb{\beta}$ due to a basis set incompleteness. This is the reason why a frequency-dependent gauge-including AO (GIAO) basis set[8] has been adopted for benchmarking purposes since the GIAO $\mathbb{\beta}$ has the same transformation properties upon a change of the coordinate origin as does the exact OR tensor.[9] Alternatively, a 'velocity-gauge' formalism can be employed in which the tensors $\mathbb{\beta}$ and $\mathbb{A}$ are calculated with a derivative operator in place of the electronic coordinate vector. For details see Reference 5. However, in order to avoid a situation where a detailed analysis is impacted too strongly by terms arising from basis set incompleteness, the basis set adopted in the calculations should be sufficiently flexible such that the GIAO terms in Equation (1) (main manuscript) are small for a molecule centered at the coordinate origin (here, the center of nuclear charges, CNC).

Table S1: Isotropic optical rotation parameter β for norbornenone calculated with GIAOs and regular field-independent AOs using length gauge (GIAO-length), and with AOs (AO-length) and with a modified velocity gauge (MVG), at 355, 589.3, and 633 nm, and at the static limit (∞ nm). [a]

β_{iso} / a.u.	GIAO-length				AO-length				MVG		
Method / λ (nm)	355	589.3	633	∞	355	589.3	633	∞	355	589.3	633
HF	-3.182	-1.670	-1.606	-1.266	-3.165	-1.661	-1.597	-1.259	-3.129	-1.640	-1.576
LC-PBE0	-5.957	-2.310	-2.195	-1.631	-5.925	-2.297	-2.182	-1.621	-5.864	-2.268	-2.154
LC-PBE0*	-5.920	-2.380	-2.263	-1.687	-5.887	-2.366	-2.249	-1.676	-5.820	-2.334	-2.219
B3LYP	-11.61	-3.340	-3.138	-2.198	-11.55	-3.318	-3.117	-2.184	-11.42	-3.272	-3.073
PBE	-36.97	-4.999	-4.617	-2.982	-36.77	-4.968	-4.589	-2.963	-36.22	-4.882	-4.508

[a] aug-cc-pVDZ basis, CNC coordinates. LC-PBE0* is the optimally tuned functional as determined in this work. See computational details regarding the other functionals. MVG implementation calculates $\omega\beta$ directly and therefore no static limit is available.

In this case, physically meaningful conclusions can be drawn about the origin of the optical rotation of a molecule based on Equation (1) (main manuscript) without trying to interpret terms that would vanish in a complete basis set limit. Tables S1, S2, and S3 demonstrate that this is the case for norbornenone in our calculations. Further, the comparison with calculations using a modified velocity gauge[10] show good agreement with the GIAO- and AO-length data. Since the sensitivity to the functional far exceeds the deviations between the GIAO-length, AO-length, and AO-velocity results, the aug-cc-pVDZ basis appears to be sufficiently flexible for the purpose of this study.

Table S2: GIAO- and AO-length components of the optical tensor $\not\beta$, in au, calculated for norbornenone with B3LYP/aug-cc-pVDZ at the sodium D-line wavelength ($\omega = 0.07732$ au).

	GIAO-length			AO-length		
			$\not\beta$			
	11	22	33	11	22	33
11	10.80	-19.86	5.673	10.64	-19.63	5.658
22	19.07	1.680	-12.59	18.87	1.689	-12.49
33	-6.507	14.77	-22.50	-6.507	14.66	-22.28

Table S3: Selected dominant canonical and localized MO (CMO and LMO) contributions to β_{33}, in au, from GIAO- and AO-length B3LYP/aug-cc-pVDZ calculations at the sodium D-line wavelength ($\omega = 0.07732$ au).

	LMO			CMO	
	GIAO	AO		GIAO	AO
πLP(O)	-4.265	-4.236	HOMO	-23.31	-23.14
$\sigma(C_1\text{-}C_2)$	-3.667	-3.639	HOMO-1	6.497	6.474
$\sigma(C_2\text{-}C_3)$	-3.282	-3.262	HOMO-2	-2.783	-2.745
$\pi(C_3\text{-}C_4)$	-5.991	-5.925	HOMO-3	-2.221	-2.210
$\sigma(C_3\text{-}C_4)$	-1.047	-1.039	HOMO-4	0.8010	0.7865
$\sigma(C_2\text{-}C_7)$	2.292	2.277	HOMO-5	1.654	1.622
$\sigma(C_7\text{-}H)$	-1.374	-1.380	HOMO-6	-0.4066	-0.4072
$\sigma(C_1\text{-}C_6)$	-1.249	-1.237	HOMO-7	-1.357	-1.338
			HOMO-8	-1.542	-1.526

Optimal tuning of the PBE-based range-separated hybrid. Chiroptical data for the 'tuned' set of functionals

We use the following 3-parameter expression for the inverse interelectronic distance in the exchange functional:[11]

$$\frac{1}{r_{12}} = \frac{\alpha + \beta\,\mathrm{erf}(\gamma r_{12})}{r_{12}} + \frac{1 - [\alpha + \beta\,\mathrm{erf}(\gamma r_{12})]}{r_{12}} \tag{6}$$

where the first term on the right-hand side is used for the long-range HF part. In Equation (6), γ is the range-separation parameter, α is the HF fraction at very small interelectronic distances, and $\alpha + \beta$ quantifies the fraction of HF exchange in the asymptotic limit at large interelectronic separations. A global hybrid such as B3LYP corresponds to $\beta = 0$, with α being the HF fraction of exchange in the functional.

We consider a range-separated hybrid variant of the PBE functional which satisfies the correct asymptotic behavior of the XC potential. It follows that $\alpha + \beta = 1$. Further, the functional is tuned to satisfy $-\varepsilon^{\mathrm{HOMO}}(N) = \mathrm{IP}(N)$ subject to the $\alpha + \beta = 1$ constraint. Following Reference 12, we minimize

$$J^2 = \sum_{i=0}^{1} [\varepsilon^{\mathrm{HOMO}}(N+i) + \mathrm{IP}(N+i)]^2 \tag{7}$$

to satisfy the IP condition simultaneously for the system with N and $N+1$ electrons, where $\mathrm{IP}(N) = E(N) - E(N-1)$ is calculated as a difference of total energies. This optimization is performed in the $\alpha = 1 - \beta$ vs. γ plane, which is the reason why the procedure is referred to as a 'two-dimensional' tuning here. The tuning was accomplished as follows. Hartree-Fock molecular orbitals were calculated for the neutral (N electrons), anion ($N+1$), and cation ($N-1$) systems. These molecular orbital vectors were then used as initial guesses for DFT calculations with the PBE0 global hybrid functional. The PBE0 molecular orbital vectors were used as input for calculations with α between 0 and 0.5 and γ between 0 and 0.5 on the tuning grid. MOs from calculations with $\alpha = 0.5$ and a given γ were used as initial guesses for calculations with α ranging from 0.6 to 0.8 and the same value of γ in order to improve convergence of the self-consistent field (SCF) procedure. Finally, for sets $\{\alpha, \beta = 1 - \alpha, \gamma\}$ satisfying the IP condition, we investigate the DFT delocalization error, quantified by the curvature of $E(N)$.

Figure S1 (panel a) shows a contour plot of J^2 in the $\alpha - \gamma$ plane. There is a continuous range of parametrizations that satisfy $J^2 \approx 0$, numerically, indicated by the thick curved line in the contour plot. Based on the IP criterion, these functionals are therefore all equally well-tuned. The $E(N)$ plot in the same figure (panel b) for a selected set of 7 parametrizations along the minimum

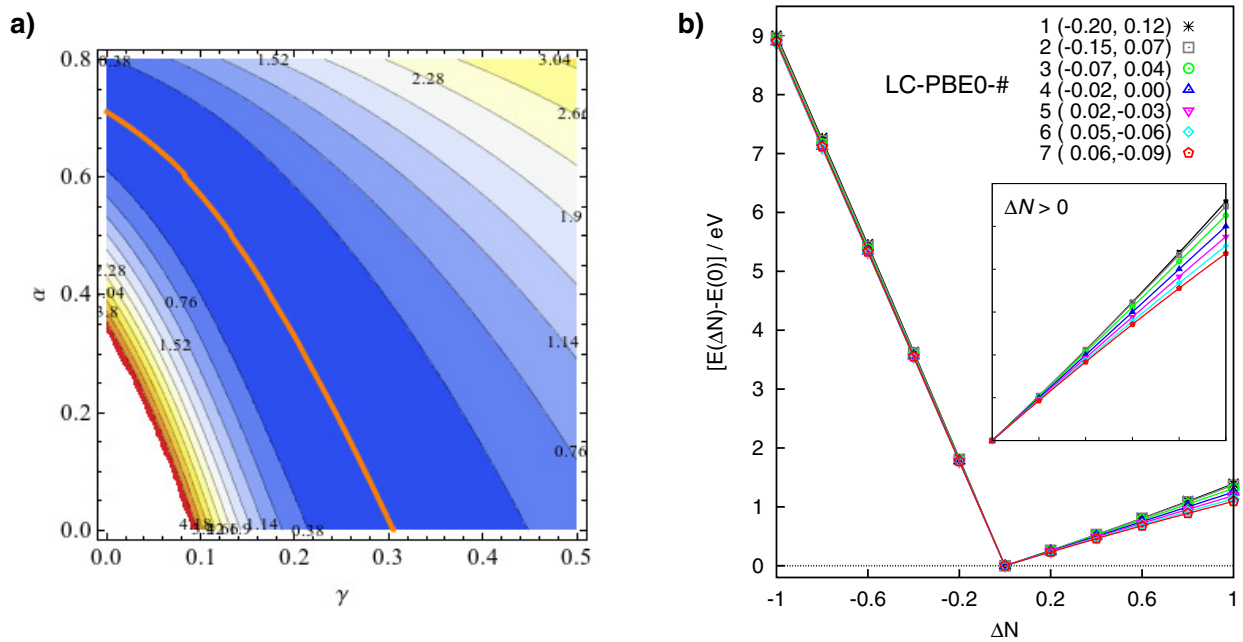

Figure S1: a) Contour plot of J^2 as a function of α and γ. The thick orange line corresponds to $J^2 \approx 0$. b) Energy of norbornenone as a function of fractional electron number, ΔN, relative to neutral system ($\Delta N = 0$) for tuned LC-PBE0-# parameterizations. The numerical values in parentheses correspond to $(\Delta N)^2$ coefficients of quadratic fits to $E(N)$ in the electron-deficient and electron-rich regime, respectively ($\Delta N < 0$, $\Delta N > 0$). The inset shows the $E(N)$ behavior in the electron-rich regime.

path of J^2 further indicates that there is some difference in the DFT delocalization error among the different parametrizations. Parametrization no. 4 appears to be the most suitable in terms of eliminating the DFT delocalization error for norbornenone. We refer to this parametrization as LC-PBE0*. Calculated chiroptical properties for a selected set of 7 parametrizations for which $J^2 \approx 0$ are collected in Table S4. For LC-PBE0*, the data are shown in Table 1.

Table S4: Tuned functional parametrizations, LC-PBE0-#, first electronic vertical excitation, and molar rotation data for norbornenone. [a]

#	$\alpha = 1 - \beta$	γ	E	$-R$	$-[\phi]_\lambda$		
					355	589.3	633
1	0.711	0.00	4.61	43.2	4531	769.9	638.2
2	0.654	0.05	4.54	43.7	4922	807.9	668.8
3	0.570	0.10	4.46	44.3	5529	861.3	711.5
4 [b]	0.461	0.15	4.36	44.5	6305	920.0	758.2
5	0.330	0.20	4.27	43.8	7165	972.8	799.7
6	0.180	0.25	4.18	42.4	8010	1012	829.8
7	0.017	0.30	4.11	40.4	8721	1032	844.9
LC-PBE0 [c]	0.250	0.30	4.29	39.1	6345	893.0	735.3
CC2 [d]			4.26	37.6	—	1081 / 879.2	—
					(6699)	(880.6)	(721.4)
CCSD [d]			4.30	23.1	—	800.9 / 602.9	—
					(4213)	(605.5)	(498.3)
Expt. [e]			4.02	51	—	1239	—

[a] Compare Fig. S1. Energy E in eV. Rotatory strength R in 10^{-40} esu^2 cm^2. Molar rotation at specified wavelengths λ in nm, $[\phi]$, in deg cm^2 / dmol. [b] Optimal parametrization as determined in this work, LC-PBE0*. [c] Stock parametrization. [d] Velocity aug-cc-pVDZ(C, O)+cc-pVDZ(H) E and R values from Ref. 13. Length (LG) / modified velocity gauge (MVG) aug-cc-pVDZ(C, O)+cc-pVDZ(H) $[\phi]$ results from References 13–15. In parentheses MVG aug-cc-pVDZ $[\phi]$ values from Ref. 16 are listed. [e] Solution data. E and R values from Ref. 17. $[\phi]$ value from Ref. 18.

Analysis of Optical Rotation for Norbornenone: Additional Data

Table S5: Composition of selected LMOs of norbornenone in terms of weight from atomic hybrids at different centers.[a]

	$\sigma(C_1\text{-}C_2)$					$\sigma(C_2\text{-}C_3)$			
	C_1	C_2	C_3+C_4	C_6	O	C_2	C_3	C_4	C_1
HF	47.0	51.4	0.669	0.190	0.202	50.5	47.6	0.316	0.652
LC-PBE0	46.7	51.5	0.860	0.170	0.187	50.7	47.1	0.314	0.775
LC-PBE0*	46.7	51.5	0.864	0.173	0.190	50.6	47.2	0.316	0.778
B3LYP	46.8	51.5	0.956	0.173	0.189	50.6	47.1	0.319	0.861
PBE	46.6	51.4	1.13	0.172	0.184	50.6	46.8	0.328	0.967

[a] Numerical data obtained from 'natural LMOs' generated by the NBO program. All values in percent. Atom numbering as in Figure 5.

Table S6: Diagonal components of the optical tensors $\mathbb{\beta}$, $\mathbb{B}$, and $\tilde{\mathbb{B}}$, in au, calculated at the static limit and sodium D-line in the coordinate system where the the chiroptical response tensor $\tilde{\mathbb{B}}$ is diagonal. 'iso' indicates the isotropic values.

ω (au) / λ (nm)	0 / ∞				0.07732 / 589.3			
Component	11	22	33	iso	11	22	33	iso
$\mathbb{\beta}$								
HF	10.73	-0.0637	-14.46	-1.266	11.95	-0.0344	-16.93	-1.670
LC-PBE0	9.875	0.4111	-15.18	-1.631	10.96	0.6124	-18.50	-2.310
LC-PBE0*	9.837	0.4526	-15.35	-1.687	10.91	0.6745	-18.73	-2.381
B3LYP	9.802	1.045	-17.44	-2.198	10.80	1.680	-22.50	-3.340
PBE	9.826	1.647	-20.42	-2.982	10.74	3.006	-28.74	-4.999
$\mathbb{B}$								
HF	5.837	-0.1962	-9.440	-1.266	6.643	-0.2156	-11.44	-1.670
LC-PBE0	5.894	0.2782	-11.06	-1.631	6.748	0.3948	-14.07	-2.310
LC-PBE0*	5.905	0.3398	-11.31	-1.687	6.754	0.4834	-14.38	-2.381
B3LYP	6.101	0.9119	-13.61	-2.198	7.021	1.393	-18.43	-3.340
PBE	6.584	1.487	-17.02	-2.982	7.705	2.507	-25.21	-4.999
$\tilde{\mathbb{B}}$								
HF	-4.818	-1.802	2.820	-1.266	-5.827	-2.398	3.214	-1.670
LC-PBE0	-5.393	-2.585	3.086	-1.631	-6.840	-3.663	3.572	-2.310
LC-PBE0*	-5.483	-2.700	3.122	-1.687	-6.949	-3.814	3.619	-2.381
B3LYP	-6.348	-3.753	3.506	-2.198	-8.520	-5.706	4.207	-3.340
PBE	-7.764	-5.216	4.035	-2.982	-11.35	-8.752	5.106	-4.999

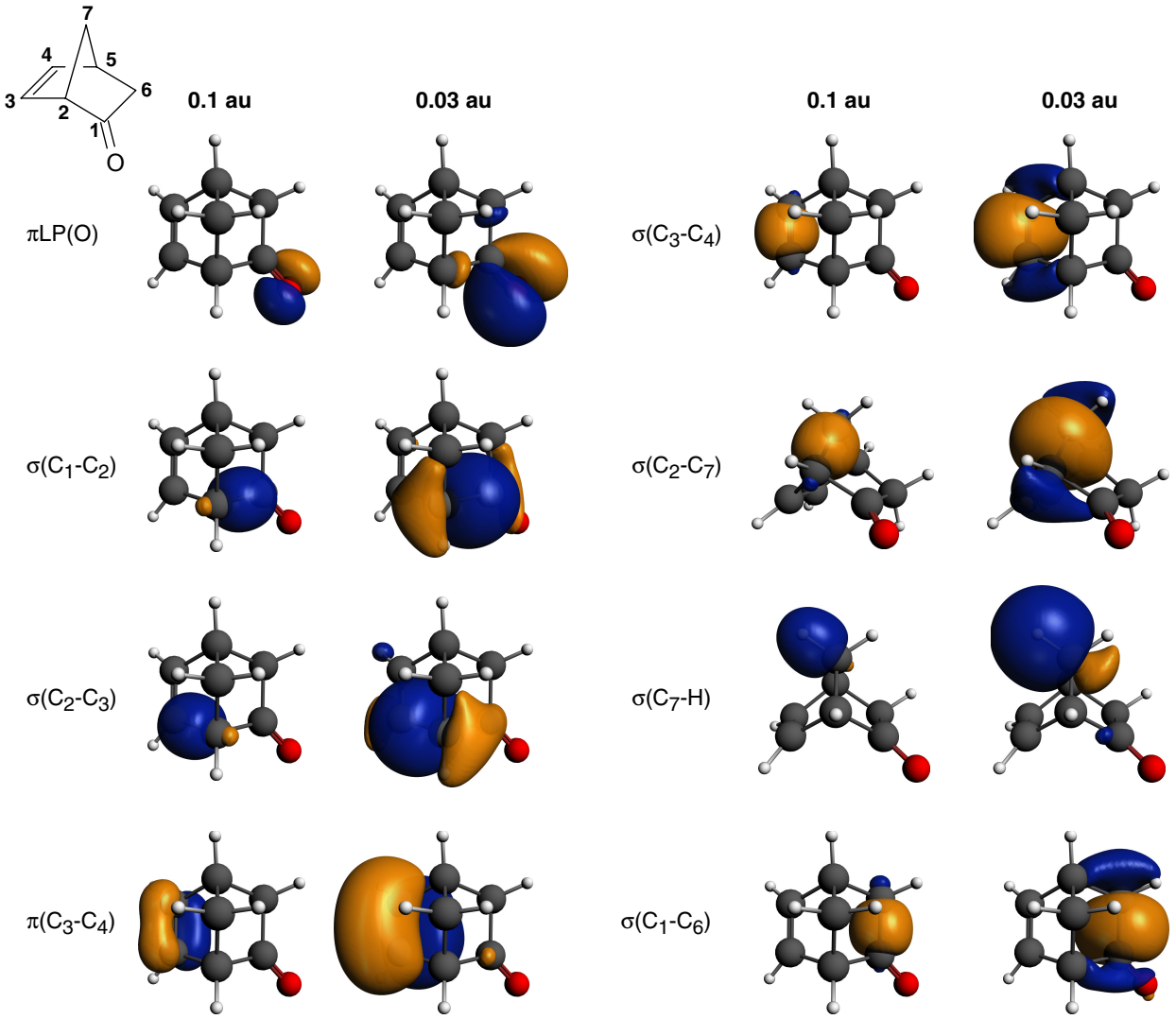

Figure S2: Isosurfaces (0.1 and 0.03 au) of selected LMOs in norbornenone.

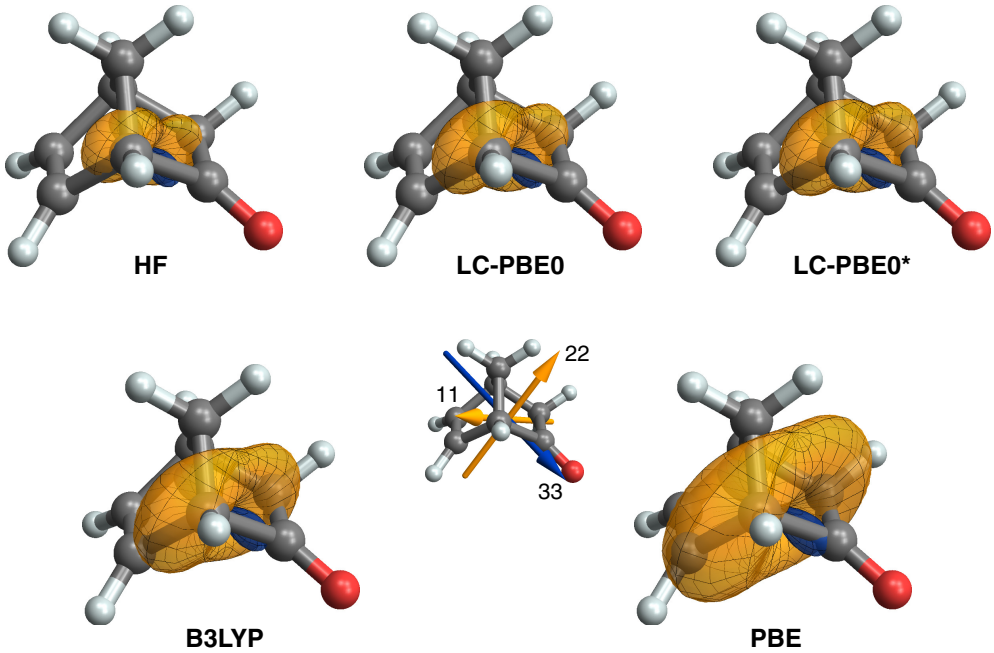

Figure S3: Polar plots of the chiroptical response tensor ($\tilde{\mathcal{B}}$) for norbornenone calculated with HF and different XC functionals at $\omega = 0$ a.u. Yellow and blue indicate negative and positive optical rotation for a given direction of the light beam. Surfaces were scaled to 30 pm per atomic unit. The principal axis system for LC-PBE0* is shown in the center. The origin is located at the CNC.

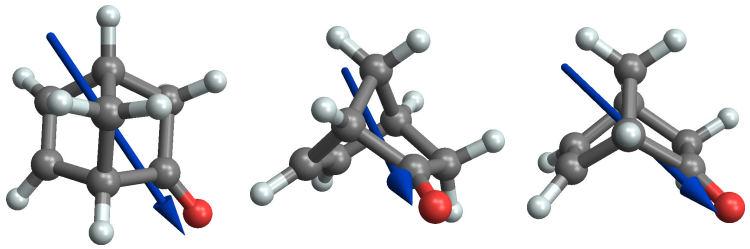

Figure S4: Principal axis 33 direction of the chiroptical response tensor at $\omega = 0$ shown for different views of norbornenone.

Table S7: Selected dominant CMO contributions to β_{33}, in au, for tested methods at the static limit and Na D-line. [a]

	Static limit ω = 0 au					Sodium D-line ω = 0.07732 au				
	HF	LC-PBE0	LC-PBE0*	B3LYP	PBE	HF	LC-PBE0	LC-PBE0*	B3LYP	PBE
HOMO	-13.36	-15.10	-16.00	-17.98	-20.02	-15.40	-18.29	-19.29	-23.31	-28.92
HOMO-1	4.543	5.152	5.894	5.984	5.078	4.422	5.258	6.048	6.497	5.896
HOMO-2	-1.595	-2.226	-2.144	-2.614	-3.150	-1.706	-2.367	-2.278	-2.783	-3.324
HOMO-3	-1.886	-1.922	-2.035	-2.077	-2.132	-2.012	-2.040	-2.161	-2.221	-2.313
HOMO-4	0.9979	0.1868	0.5837	0.7472	0.1366	1.016	0.2053	0.6132	0.8010	0.2056
HOMO-5	2.429	1.602	1.796	1.649	1.337	2.468	1.634	1.824	1.654	1.292
HOMO-6	-2.345	-0.0698	-0.5793	-0.3867	0.4545	-2.418	-0.0736	-0.5995	-0.4066	0.4535
HOMO-7	-1.155	-1.402	-1.420	-1.345	-1.132	-1.171	-1.434	-1.442	-1.357	-1.123
HOMO-8	-1.857	-1.526	-1.597	-1.542	-1.294	-1.895	-1.553	-1.625	-1.542	-1.253
Σ(H-8 to H)	-14.23	-15.30	-15.50	-17.56	-20.73	-16.70	-18.66	-18.91	-22.67	-29.09
Σ(H-28 to H-9)	-0.2329	0.1226	0.1489	0.1207	0.3083	-0.2332	0.1589	0.1814	0.1645	0.3469

[a] Compare Figures S5, S6, S9, and S10 for representative isosurface plots.

Table S8: Selected dominant LMO contributions to β_{33}, in au, for tested methods at the static limit and Na D-line.[a]

	Static limit $\omega = 0$					Sodium D-line $\omega = 0.07732$ au				
LMO	HF	LC-PBE0	LC-PBE0*	B3LYP	PBE	HF	LC-PBE0	LC-PBE0*	B3LYP	PBE
πLP(O)	-0.6895	-1.615	-1.583	-2.597	-4.106	-1.143	-2.576	-2.526	-4.265	-7.276
$\sigma(C_1\text{-}C_2)$	-1.994	-2.316	-2.330	-2.789	-3.184	-2.357	-2.868	-2.893	-3.667	-4.565
$\sigma(C_2\text{-}C_3)$	-2.698	-3.103	-3.027	-3.122	-3.149	-2.831	-3.258	-3.171	-3.282	-3.287
$\pi(C_3\text{-}C_4)$	-5.276	-4.780	-4.922	-4.894	-5.380	-6.197	-5.633	-5.826	-5.991	-6.908
$\sigma(C_3\text{-}C_4)$	-0.9345	-0.9611	-0.9847	-1.145	-1.229	-0.8586	-0.8703	-0.9008	-1.047	-1.119
$\sigma(C_2\text{-}C_7)$	2.045	2.290	2.265	2.371	2.426	2.001	2.237	2.211	2.292	2.283
$\sigma(C_7\text{-}H)$	-1.247	-1.256	-1.209	-1.291	-1.185	-1.293	-1.314	-1.265	-1.374	-1.287
$\sigma(C_1\text{-}C_6)$	0.0684	-0.3472	-0.2671	-0.6530	-0.9687	-0.1174	-0.7268	-0.6293	-1.249	-1.994
Σ(1-8)	-10.73	-12.09	-12.06	-14.12	-16.78	-12.80	-15.01	-15.00	-18.58	-24.15
Σ(9-29)	-3.737	-3.089	-3.292	-3.320	-3.641	-4.135	-3.491	-3.732	-3.920	-4.589
β_{33}	-14.46	-15.18	-15.35	-17.44	-20.42	-16.93	-18.50	-18.73	-22.50	-28.74
$\Sigma(\beta_{11}, \beta_{22})$	10.66	10.29	10.29	10.85	11.47	11.92	11.57	11.59	12.48	13.74

[a] Compare Figures S7, S8, S11, and S12 for representative isosurface plots.

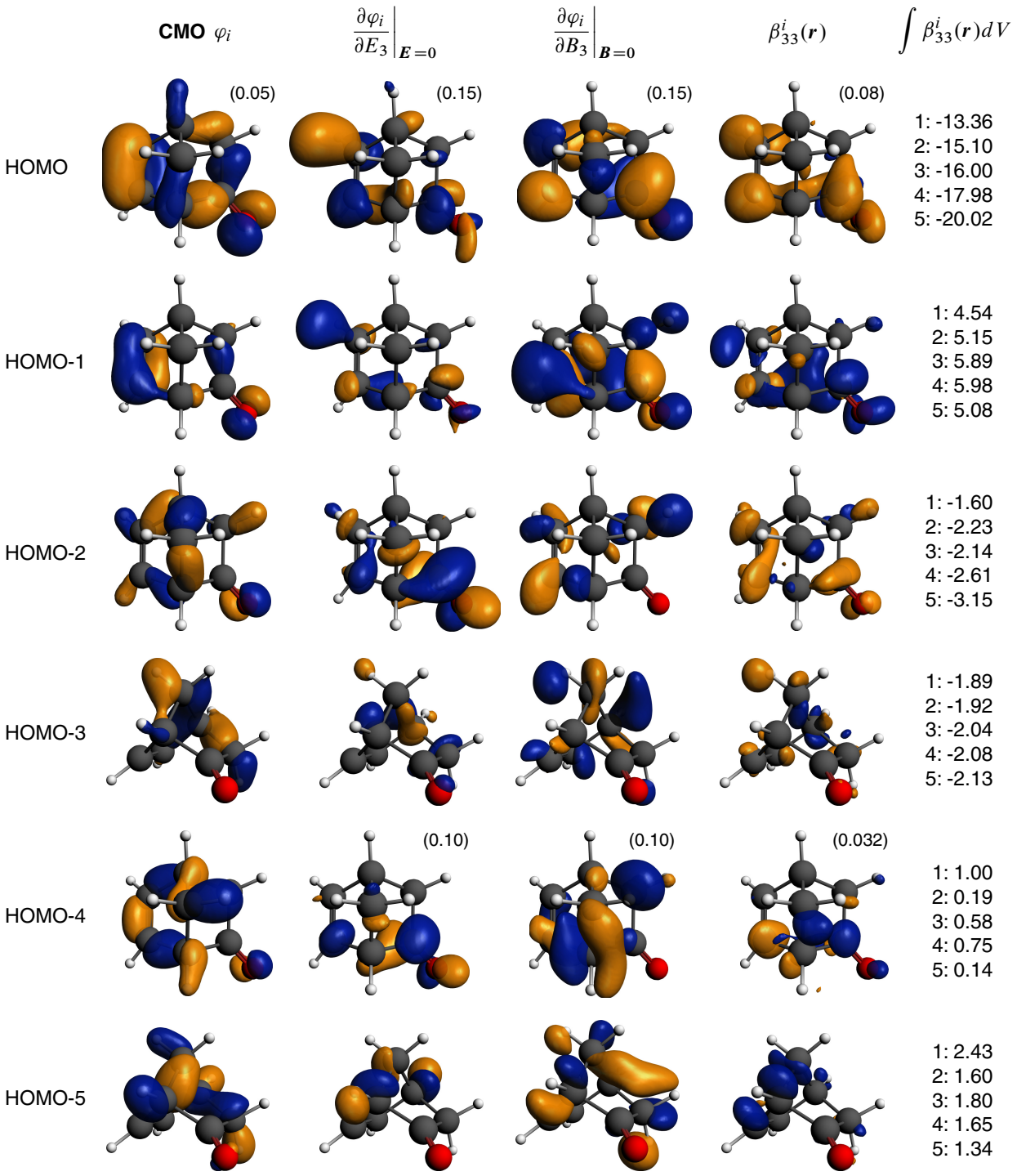

Figure S5: Selected dominant CMO (HOMO to HOMO-5) contributions to β_{33} at the static limit ($\omega = 0$ au). Numerical values listed correspond to, respectively: HF (1), LC-PBE0 (2), LC-PBE0* (3), B3LYP (4), and PBE (5). Isosurfaces presented were generated for LC-PBE0* from AO-length calculations. The contour values are (left to right) 0.08, 0.12, 0.12, and 0.04 au unless directly specified.

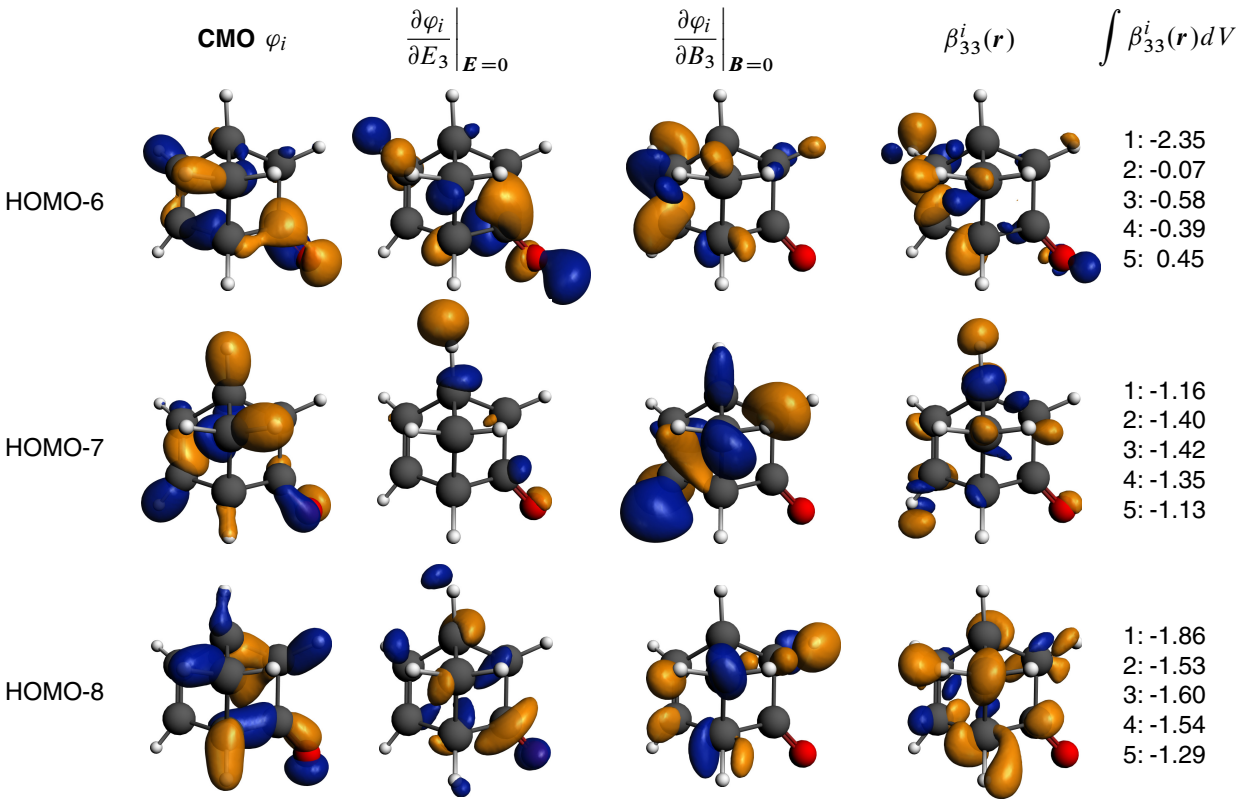

Figure S6: Selected dominant CMO (HOMO-6 to HOMO-8) contributions to β_{33} at the static limit ($\omega = 0$ au). Numerical values listed correspond to, respectively: HF (1), LC-PBE0 (2), LC-PBE0* (3), B3LYP (4), and PBE (5). Isosurfaces presented were generated for LC-PBE0* from AO-length calculations. The contour values are (left to right) 0.08, 0.1, 0.1, and 0.02 au.

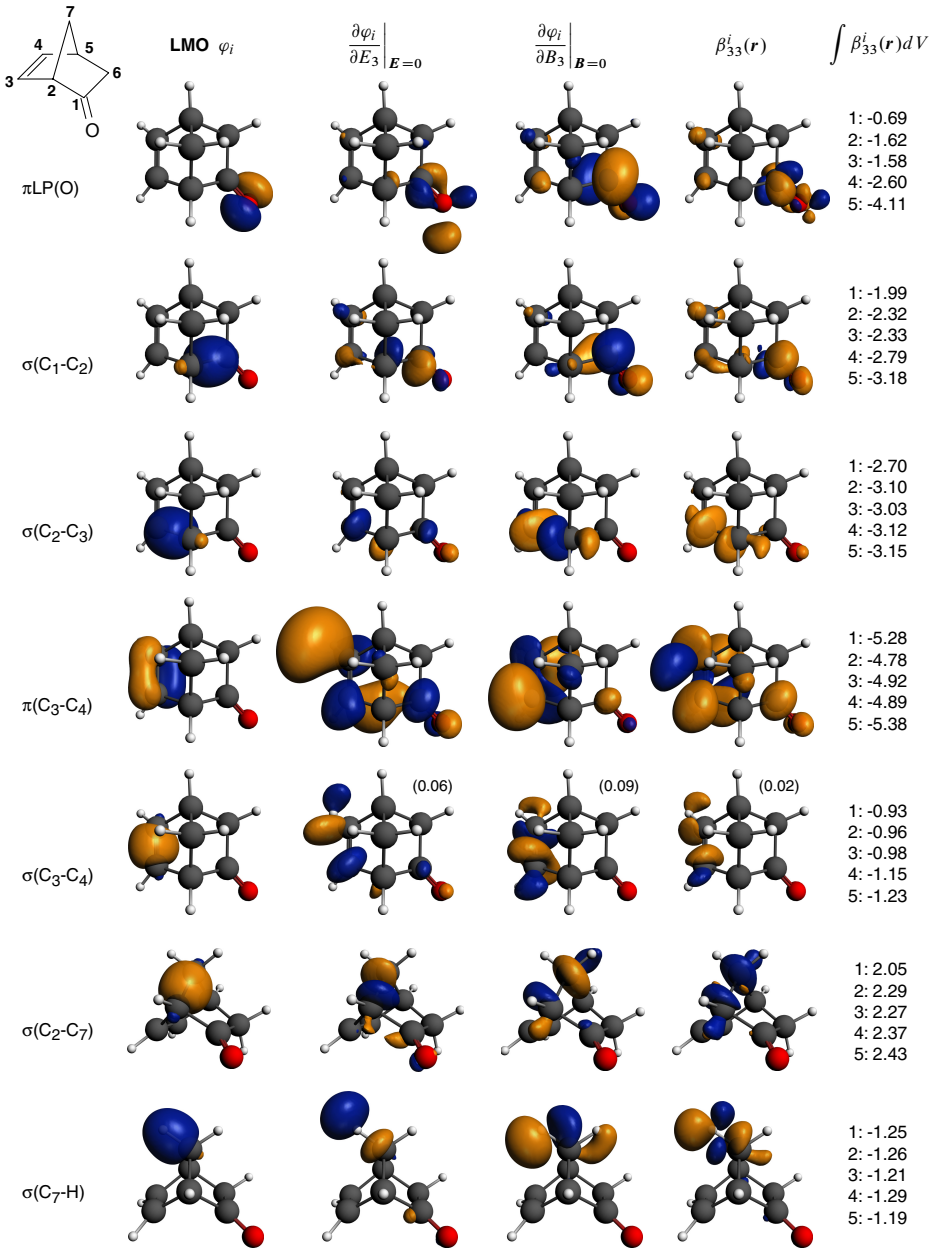

Figure S7: Selected dominant LMO contributions to β_{33} at the static limit ($\omega = 0$ au). Numerical values listed correspond to, respectively: HF (1), LC-PBE0 (2), LC-PBE0* (3), B3LYP (4), and PBE (5). Isosurfaces presented were generated for LC-PBE0* from AO-length calculations. The contour values are (left to right) 0.1, 0.12, 0.12, and 0.04 au unless directly specified.

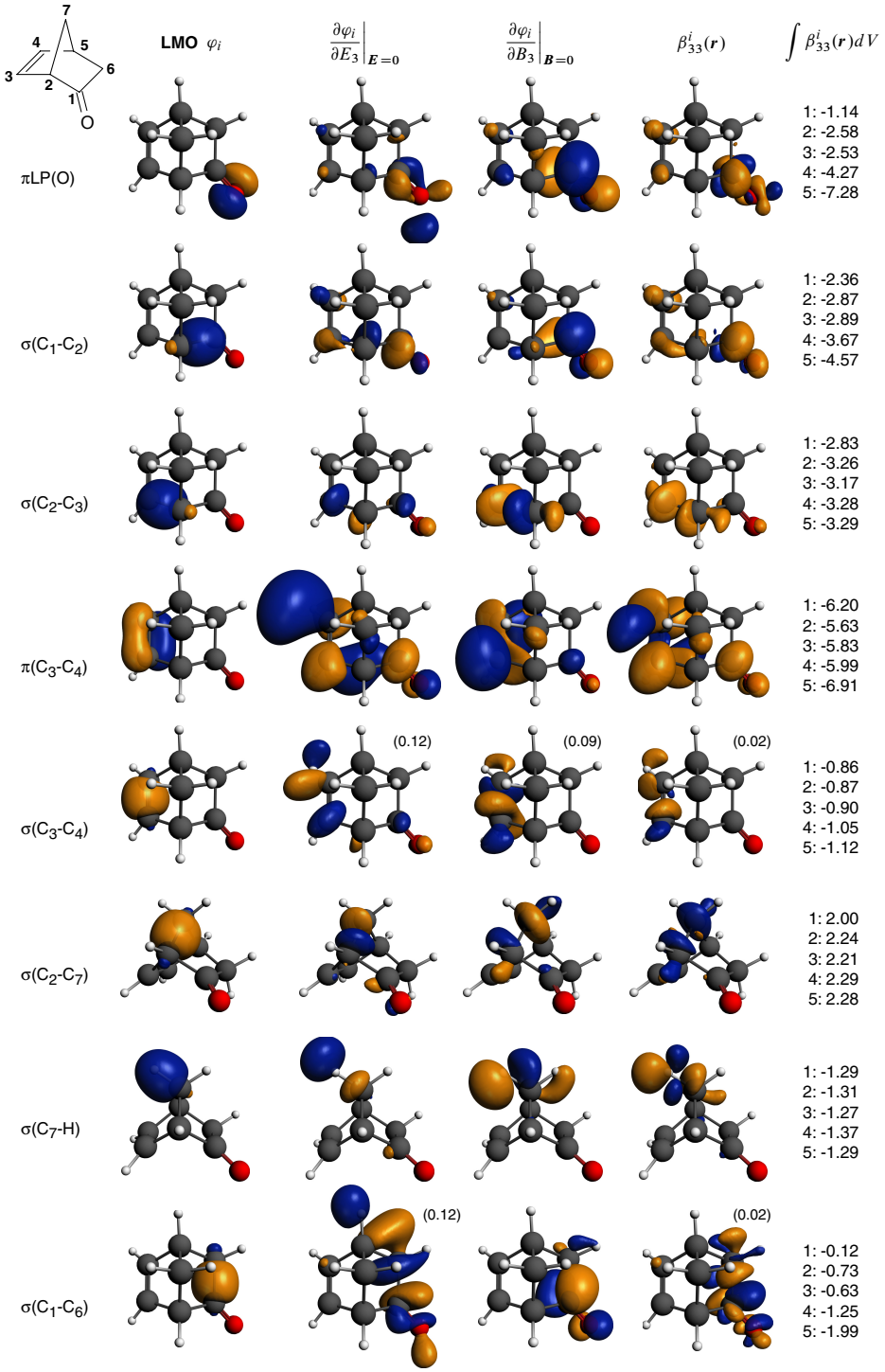

Figure S8: Selected dominant LMO contributions to β_{33} at the sodium D-line wavelength ($\omega =$ 0.07732 au). Numerical values listed correspond to, respectively: HF (1), LC-PBE0 (2), LC-PBE0* (3), B3LYP (4), and PBE (5). Isosurfaces presented were generated for LC-PBE0* from AO-length calculations. The contour values are (left to right) 0.1, 0.25, 0.12, and 0.04 au unless directly specified. The E-field derivatives shown here are the sums of the two derivatives in Eq. (1) (main manuscript).

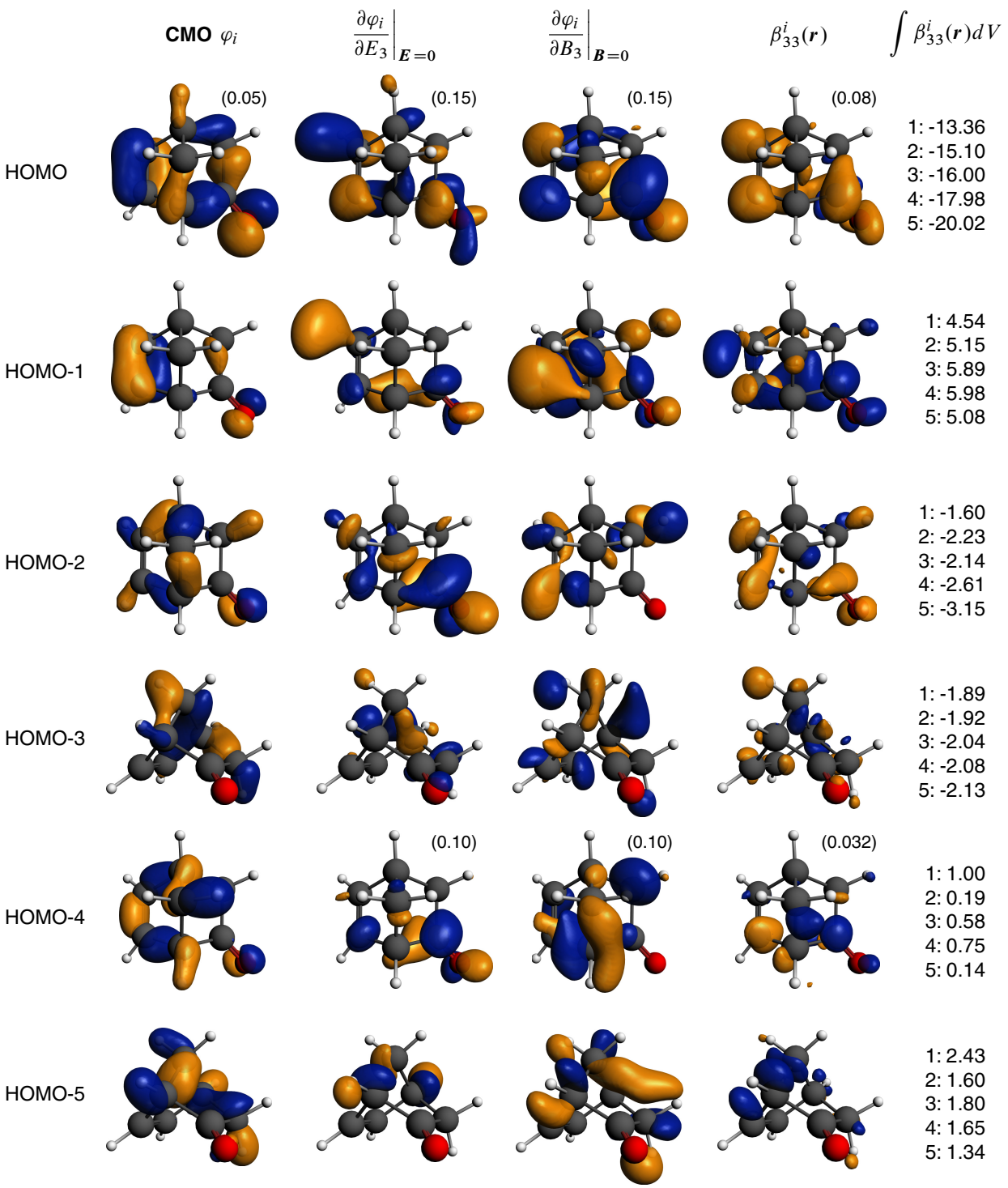

Figure S9: Selected dominant CMO (HOMO to HOMO-5) contributions to β_{33} at the static limit ($\omega = 0$ au). Numerical values listed correspond to, respectively: HF (1), LC-PBE0 (2), LC-PBE0* (3), B3LYP (4), and PBE (5). Isosurfaces presented were generated for B3LYP from AO-length calculations. The contour values are (left to right) 0.08, 0.12, 0.12, and 0.04 au unless directly specified.

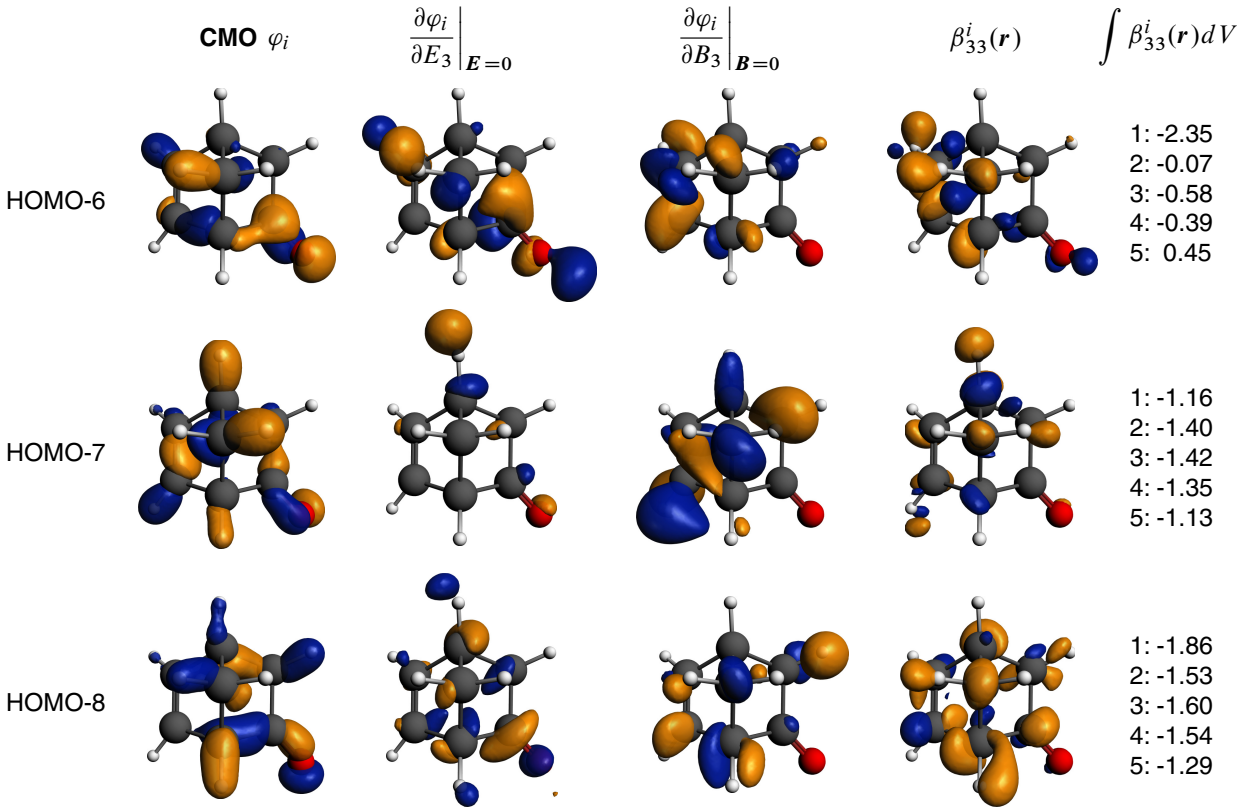

Figure S10: Selected dominant CMO (HOMO-6 to HOMO-8) contributions to β_{33} at the static limit ($\omega = 0$ au). Numerical values listed correspond to, respectively: HF (1), LC-PBE0 (2), LC-PBE0* (3), B3LYP (4), and PBE (5). Isosurfaces presented were generated for B3LYP from AO-length calculations. The contour values are (left to right) 0.08, 0.1, 0.1, and 0.02 au.

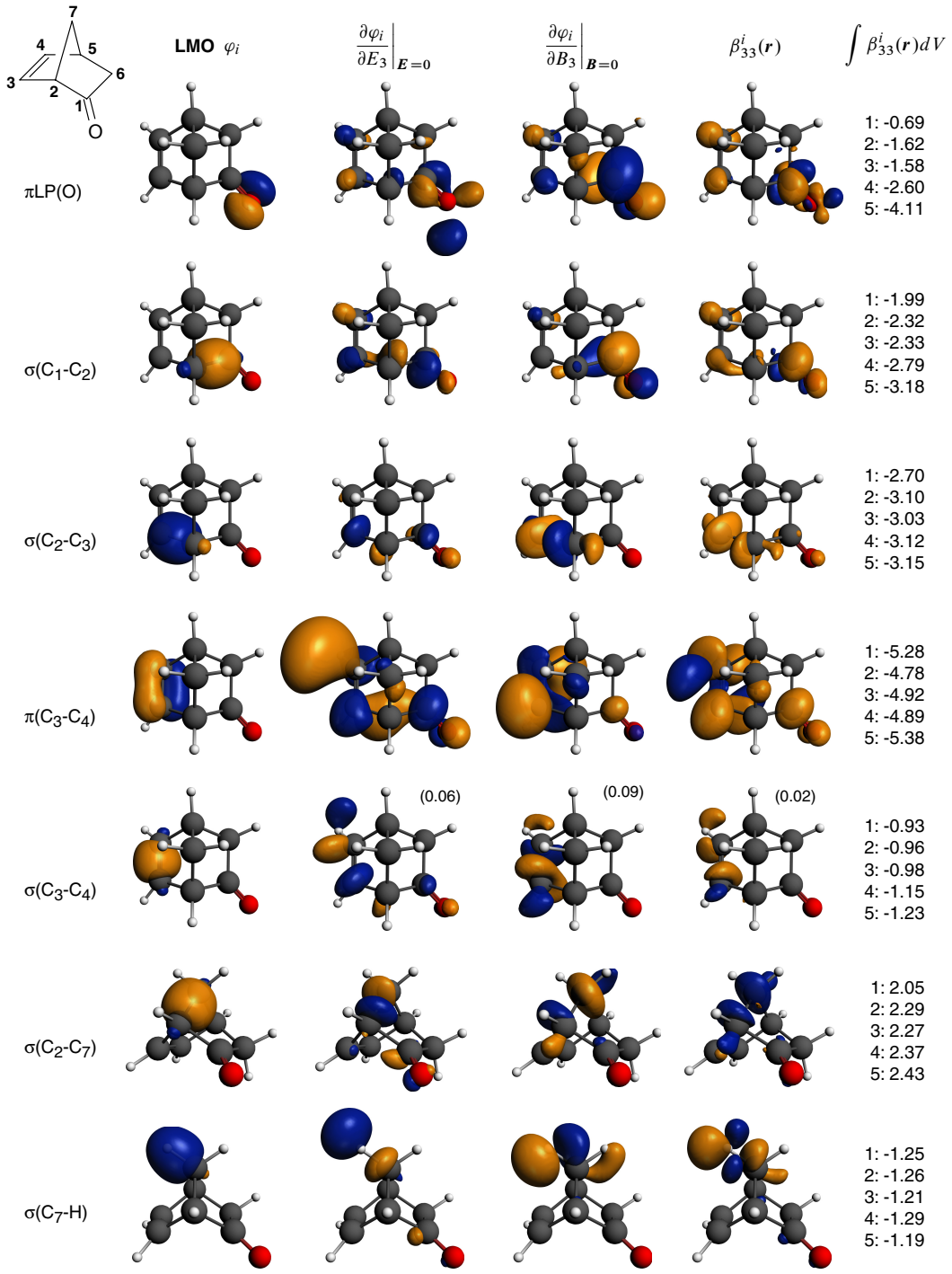

Figure S11: Selected dominant LMO contributions to β_{33} at the static limit ($\omega = 0$ au). Numerical values listed correspond to, respectively: HF (1), LC-PBE0 (2), LC-PBE0* (3), B3LYP (4), and PBE (5). Isosurfaces presented were generated for B3LYP from AO-length calculations. The contour values are (left to right) 0.1, 0.12, 0.12 , and 0.04 au unless directly specified.

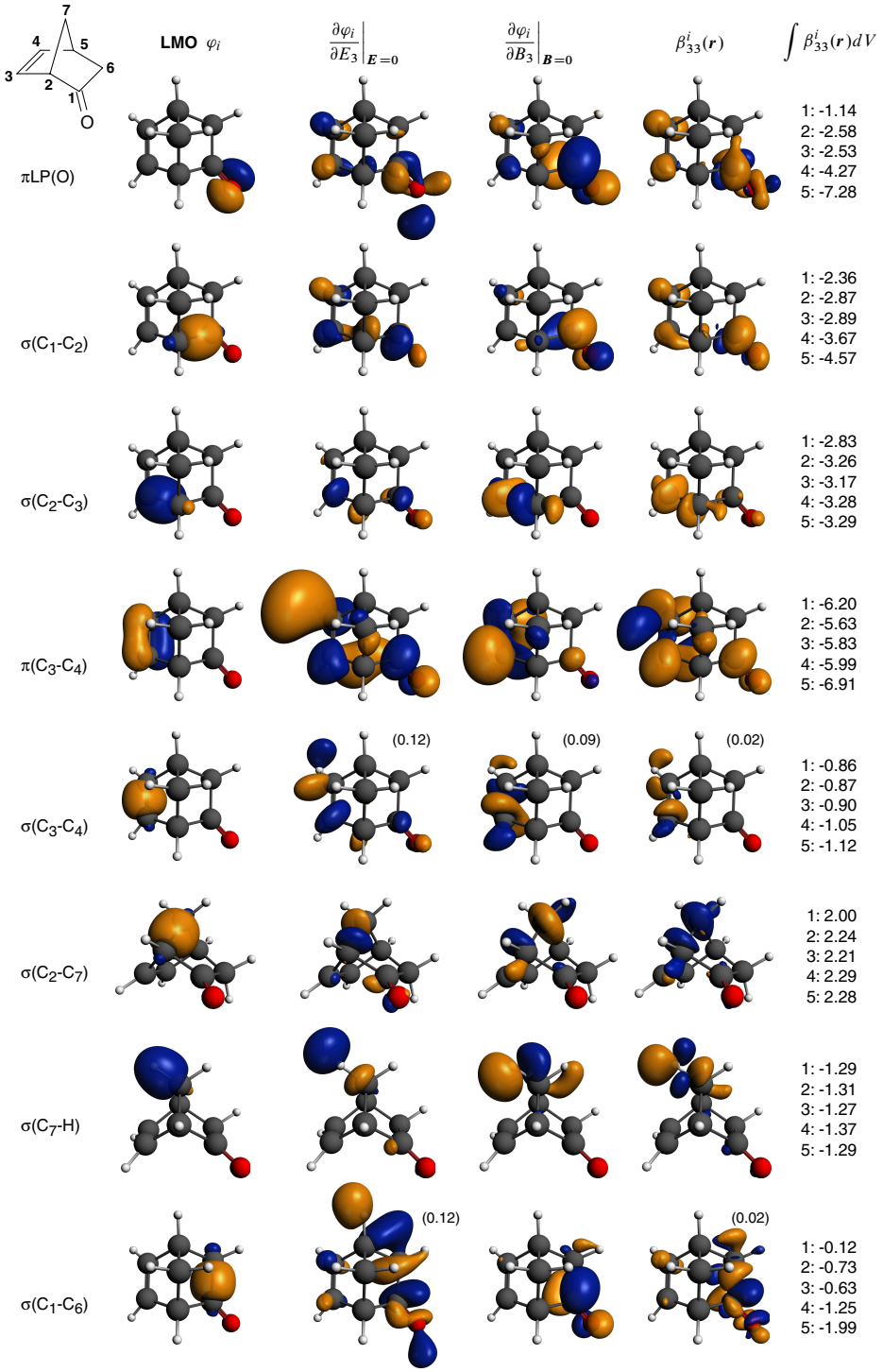

Figure S12: Selected dominant LMO contributions to β_{33} at the sodium D-line wavelength ($\omega =$ 0.07732 au). Numerical values listed correspond to, respectively: HF (1), LC-PBE0 (2), LC-PBE0* (3), B3LYP (4), and PBE (5). Isosurfaces presented were generated for B3LYP from AO-length calculations. The contour values are (left to right) 0.1, 0.25, 0.12, and 0.04 au unless directly specified. The E-field derivatives shown here are the sums of the two derivatives in Eq. (1) (main manuscript).

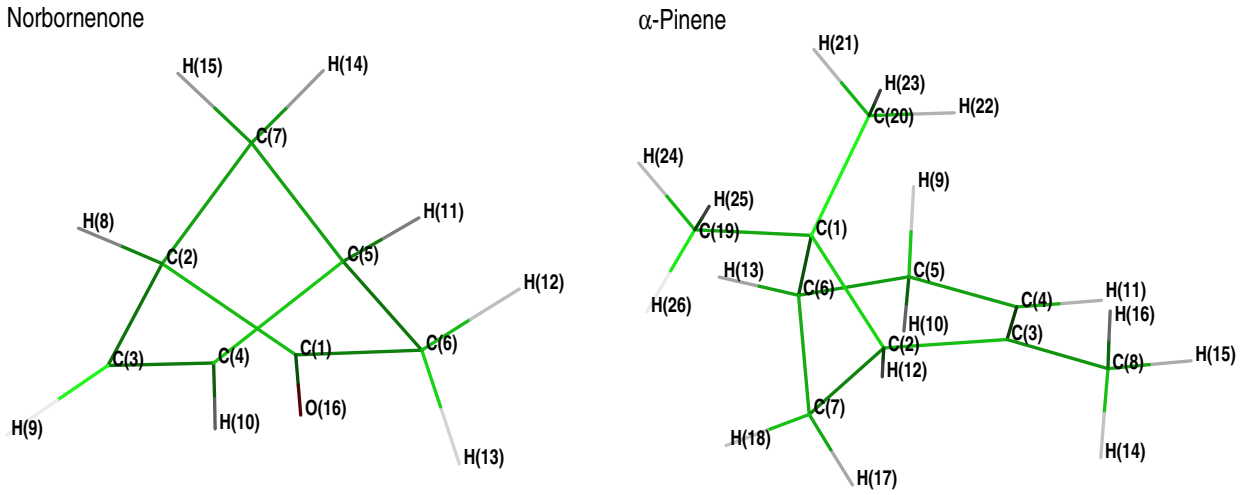

Figure S13: Numbering scheme applied in norbornenone and α-pinene molecular structures.

Table S9: LMO contributions to 11, 22, 33 components of β for norbornenone and α-pinene at the static limit. LC-PBE0* functional. Atom numbering as in Figure S13. 'CR' and 'LP' stand for core and lone-pair MOs.

	Norbornenone				α-Pinene		
LMO	11	22	33	LMO	11	22	33
Σ(CR)	0.007	0.000	0.010	Σ(CR)	0.040	-0.021	-0.004
σLP(O_{16})	0.094	-0.039	-0.051	σ(C_1-C_2)	-0.808	2.471	-1.412
σ(C_4-C_5)	2.870	-2.003	-0.794	σ(C_8-H_{16})	0.190	-1.659	1.404
σ(C_3-C_4)	1.148	-0.0888	-0.985	σ(C_7-H_{17})	1.899	0.455	-2.086
σ(C_2-H_8)	-0.0562	0.100	-0.255	σ(C_{20}-H_{21})	-1.886	1.742	0.0556
σ(C_7-H_{15})	1.522	0.0482	-1.209	σ(C_{19}-H_{24})	-1.829	2.505	-0.731
σ(C_6-H_{13})	-0.0382	0.0712	0.218	σ(C_8-H_{14})	0.0922	-0.0314	0.0372
σ(C_5-H_{11})	0.363	-0.150	-0.0871	σ(C_7-H_{18})	-0.986	1.660	-0.793
σ(C_4-H_{10})	-0.312	0.656	-0.771	σ(C_1-C_6)	0.311	0.164	-0.723
σ(C_7-H_{14})	0.516	0.116	-0.757	σ(C_4-H_{11})	0.0817	0.0642	-0.232
σ(C_1-O_{16})	0.0091	0.0425	-0.0721	σ(C_6-H_{13})	0.788	-0.736	0.267
σ(C_6-H_{12})	0.353	-0.481	-0.0354	σ(C_1-C_{20})	3.076	-1.043	-2.200
σ(C_1-C_6)	-0.383	0.398	-0.267	σ(C_5-H_9)	1.172	-0.619	-1.100
σ(C_1-C_2)	0.331	0.620	-2.330	σ(C_{20}-H_{22})	0.526	-2.542	1.602
σ(C_3-H_9)	0.987	-0.864	0.0369	σ(C_2-H_{12})	0.0257	0.159	-0.409
σ(C_2-C_3)	0.784	1.749	-3.026	σ(C_8-H_{15})	0.806	1.374	-2.032
σ(C_2-C_7)	-0.138	-1.858	2.265	σ(C_3-C_4)	1.161	-0.240	-1.001
σ(C_5-C_7)	-2.452	2.123	0.327	σ(C_3-C_8)	1.685	-1.279	-0.241
σ(C_5-C_6)	1.604	-0.824	-0.709	σ(C_{19}-H_{25})	-1.343	-0.0926	1.431
π(C_1-O_{16})	0.335	-0.132	-0.332	σ(C_{20}-H_{23})	0.323	0.969	-1.290
πLP(O_{16})	-0.217	0.510	-1.583	σ(C_1-C_{19})	0.549	-1.301	0.905
π(C_3-C_4)	2.511	0.458	-4.922	σ(C_5-C_6)	-1.698	0.166	1.852
				σ(C_4-C_5)	3.596	-1.563	-1.844
				σ(C_{19}-H_{26})	3.657	-1.961	-1.691
				σ(C_2-C_7)	0.525	-3.253	1.757
				σ(C_2-C_3)	0.641	0.754	-1.593
				σ(C_6-C_7)	0.787	-0.151	-0.425
				σ(C_5-H_{10})	1.602	0.425	-1.288
				π(C_3-C_4)	4.675	0.0738	-4.903
β	9.837	0.4526	-15.35		19.66	-3.503	-16.71
β_{iso}		-1.687				-0.184	

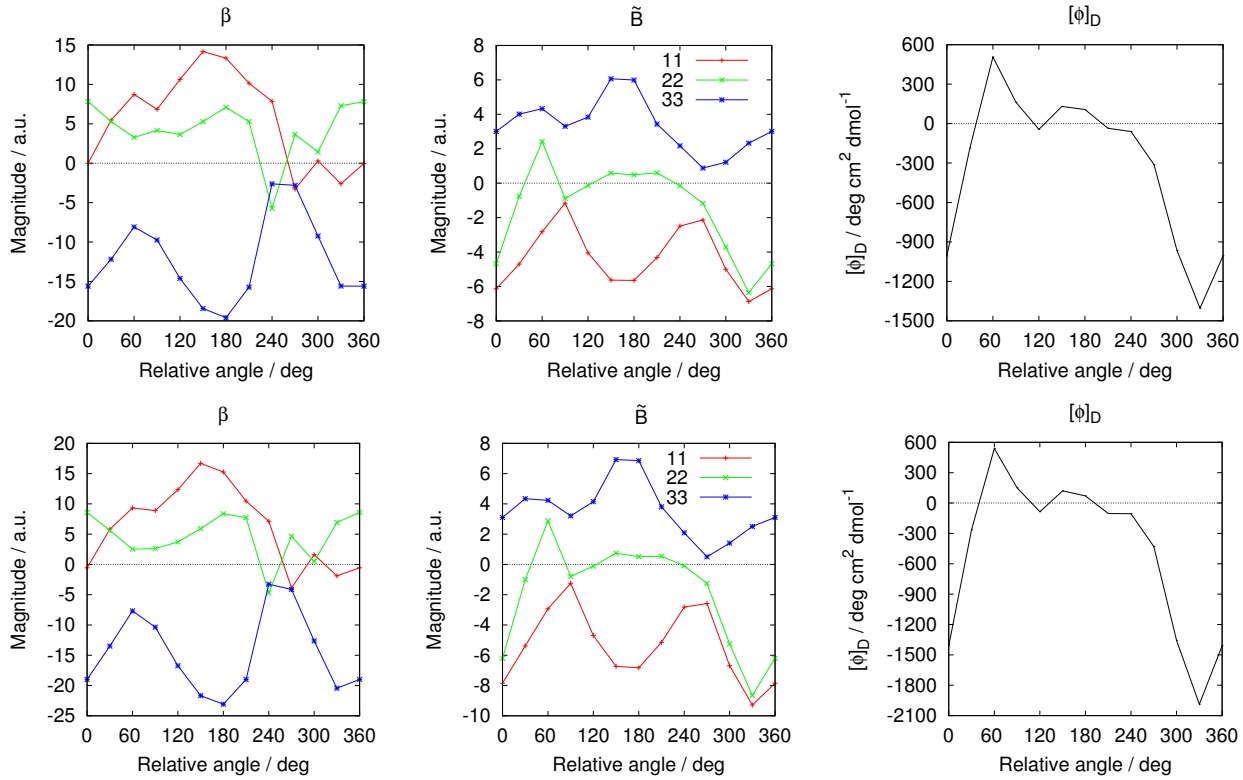

Figure S14: Chiroptical tensors for the norbornenone molecular fragment, $H_2C{=}CH{-}CH_2COH$, rotated around the C_2-C_3 bond axis in 30° increments for LC-PBE0* (top) and B3LYP (bottom). Left to right: β and $\tilde{B}$ tensor components in the 11 (red), 22 (green), and 33 (blue) directions followed by a plot of $[\phi]_D$ versus dihedral angle relative to that in norbornenone (289.6°).

References

[1] Autschbach, J. *ChemPhysChem* **2011,** *12,* 3224-3235.

[2] Graham, E. B.; Raab, R. E. *Proc. R. Soc. Lond. A* **1990,** *430,* 593-614.

[3] Buckingham, A. D.; Dunn, M. B. *J. Chem. Soc. A* **1971,** 1988-1991.

[4] Barron, L. D. *Molecular light scattering and optical activity;* Cambridge University Press: 2nd ed.; 2004.

[5] Krykunov, M.; Autschbach, J. *J. Chem. Phys.* **2006,** *125,* 034102-10.

[6] Autschbach, J. *Chirality* **2009,** *21,* E116-E152.

[7] Autschbach, J.; Nitsch-Velasquez, L.; Rudolph, M. *Top. Curr. Chem.* **2011,** *298,* 1-98.

[8] Krykunov, M.; Autschbach, J. *J. Chem. Phys.* **2005,** *123,* 114103-10.

[9] Bak, K. L.; Hansen, A. E.; Ruud, K.; Helgaker, T.; Olsen, J.; Jørgensen, P. *Theor. Chim. Acta* **1995,** *90,* 441-458.

[10] Pedersen, T. B.; Koch, H.; Boman, L.; Sánchez de Merás, A. M. J. *Chem. Phys. Lett.* **2004,** *393,* 319-326.

[11] Yanai, T.; Tew, D. P.; Handy, N. C. *Chem. Phys. Lett.* **2004,** *393,* 51–57.

[12] Kuritz, N.; Stein, T.; Baer, R.; Kronik, L. *J. Chem. Theory Comput.* **2011,** *7,* 2408–2415.

[13] Ruud, K.; Stephens, P. J.; Devlin, F. J.; Taylor, P. R.; Cheeseman, J. R.; Frisch, M. J. *Chem. Phys. Lett.* **2003,** *373,* 606–614.

[14] Crawford, T. D.; Tam, M. C.; Abrams, M. L. *J. Phys. Chem. A* **2007,** *111,* 12057-68.

[15] Crawford, T. D.; Stephens, P. J. *J. Phys. Chem. A* **2008,** *112,* 1339-1345.

[16] Mach, T. J.; Crawford, T. D. *J. Phys. Chem. A* **2011,** *115,* 10045–10051.

[17] Lightner, D. A.; Beavers, W. A. *J. Am. Chem. Soc.* **1971,** *93,* 2677–2684.

[18] Lightner, D. A.; Gawronski, J. K.; Bouman, T. D. *J. Am. Chem. Soc.* **1980,** *102,* 5749–5754.